地震研究所彙報
Bull. Earthq. Res. Inst.
Univ. Tokyo
Vol. 78 (2003) pp. 75-82

The role of fault continuity at depth in numerical simulations of earthquake rupture

Hideo Aochi*
Laboratoire de Géologie, École Normale Supérieure Paris

submitted to Bull. Earthq. Res. Inst., Univ. Tokyo (30 November 2002, revised on 29 April 2003).

Abstract

We simulated dynamic rupture propagation along a branched fault, which is partially segmented by a slit. This is an analogy of a strike slip fault, which displays a jog structure on the ground surface but forms a continuous system at depth. We observed that rupture directivity can significantly change due to the existence of the fault slit and that the relative location of the slit to the hypocenter is important. On the other hand, final rupture area and slip distribution are principally controlled by the continuity of the fault at depth. However, if the continuous part of the fault is too narrow, the rupture can be disturbed. If enough stress is accumulated, rupture can still progress through a strong dynamic stress transfer at the bottom of the slit. This infers that it is important to reveal the fault structure at depth and its surroundings in order to discuss rupture size in a complex fault system in the geological meaning.

Key words: fault geometry, fault continuity, branch, slit, rupture propagation

1. Introduction

We are now able to treat non-planar fault geometry in dynamic modeling of earthquake rupture. It is important to introduce tectonic and geological information into model parameters: fault geometry, stress fields and friction law. In a realistic way, although we still have to simplify some of this information due to numerical limitations, it is crucial to consider how to define model parameters reasonably.

For the 1999 Izmit earthquake (M=7.4), we considered how to introduce fault geometry into a numerical simulation given insufficiency of observed fault traces [Aochi and Madariaga, 2003]. We observed that small differences in fault geometry cause significant changes in the rupture process and, as a result, in seismic wave generation. The main problem lies in fault jogs. Beneath the Sapanca lake located at the western side of the hypocenter, for example, we found that it was better to assume a continuous fault with a small bend to explain the near-field seismograms, although observed fault traces also allowed us to interpret this portion as a jog (disconnected parallel faults). For this earthquake, a continuous fault is reasonable, because this event occurred along a large plate boundary (North Anatolian fault) which should be one kinematic system from the viewpoint of tectonics.

It often appears in the case of intra-plate strike-slip faults and also in the case of thrust faults, for which the observed fault traces and the structure under the ground are not always clear. We can treat them as a continuous fault system in some cases, while we can also regard them as a disconnected system in other cases where rupture jumps from one part to another, as numerically demonstrated by Harris and Day (1993, 1999) and by Kase and Kuge (1998, 2001). However, fault structure in the field is more complicated. In fact, Aochi and Madariaga (2003) pointed out that a segmented fault geometry was better for explaining observed surface breaks. In this study, we consider a partially segmented fault as shown in Figure 1, as an analogy of a strike-slip fault,

* e-mail: hideo.aochi@irsn.fr (H. A. is now at the Institut de Radioprotection et de Sûreté Nucléaire, France; Address: IRSN/DPRE/SERGD/BERSSIN, BP 17, 92262 Fontenay-aux-Roses Cedex. France; Telephone: +33-1.58.35.82.57; Fax: +33-1.58.35.81.30)

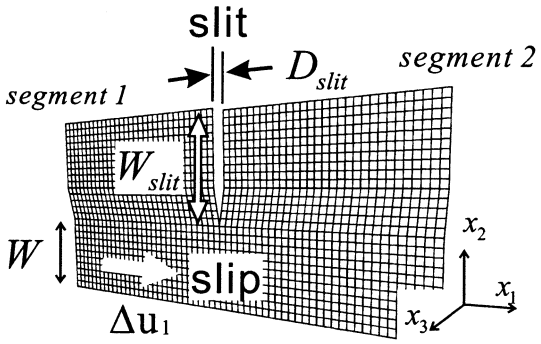

Fig. 1. Fault geometry modeled in this study. Rupture starts at the side of segment 1. Also see Table 1.

the geometry of which changes with depth. We assume the fault system is embedded in an unbounded medium. A slit partially separates the fault into the two segments. Beneath the slit the fault forms one plane. This provides the key to solving the contradiction between the discontinuitysuggested by geological surface observation and the continuity implied by tectonic and seismological analyses.

Pioneering numerical and theoretical work was done by Tada and Yamashita (1997) and Kame and Yamashita (1999), who studied a 2D case where the branching direction is the same as the slip direction (mode II, P-SV problem). This corresponds to the observed branching geometry for a strike-slip fault and for a spray fault in the case of normal/inverse faulting. The other branching direction (mode III, SH problem in two dimension) has been regarded as less important, because from the viewpoint of simple geography, a kink does not disturb mode III deformation. The discussion for a 3D problem is basically the same as the 2D one, as long as the fault structure remains isotropic in one direction [Aochi *et al.,* 2002; Kame *et al.,* 2003]. However, there are few studies concerning a fully 3D structure such as Figure 1 [e.g. Fukuyama *et al.,* 2002]. In that case, each part of the fault geometry may play an important and different role, so we have to carefully investigate the whole process.

2. Numerical Procedure

To simulate dynamic rupture propagation along a non-planar fault, we use the same boundary integral equation method (BIEM) as the one used by Aochi *et al.* (2000). Different types of BIEM have been studied in the past [e.g. Andrews, 1976a; Das and Aki, 1977]. Later, an explicit stress-velocity formulation in time domain and in real space was developed by Cochard and Madariaga (1994) for a 2D anti-plane problem. Fukuyama and Madariaga (1995, 1998) extended the formulation for a planar fault in 3D; and, finally Tada *et al.* (2000) and Aochi *et al.* (2000) worked out the 3D general case. This BIEM provides flexibility in the definition of fault geometry and the advantage of an accurate estimation of stress and slip velocity on the fault, thanks to its mathematical formulation. Our model is placed in a three-dimensional unbounded, homogeneous elastic medium. For simplicity, we fix the slip direction along the x_1 axis, assuming that uniform shear stress accumulates in this direction only.

We introduce a simple slip-weakening friction law, which controls the rupture process as given by the following relation between the shear stress τ and the fault slip Δu,

$$\tau(\Delta u)=\tau_p\left(1-\frac{\Delta u}{D_c}\right)H\left(1-\frac{\Delta u}{\mathrm{Dc}}\right) \qquad (1)$$

where τ_p and D_c are peak strength and critical slip-weakening distance, respectively. These parameters are assumed to be uniform anywhere on the fault plane except within an initial crack patch. $H(\cdot)$ represents the Heaviside step function. The model parameters are given in Table 1. Since we define the shear stress on the fault plane directly without considering any external load, the absolute levels of stress and friction have no significance in this simulation; that is, stress is reduced to zero in Equation 1 after slip exceeds D_c.

To start spontaneous dynamic rupture growth, we let one grid break artificially at the hypocenter at the first time step with an initial stress of 13 MPa. Then, until the rupture propagates outward spontaneously at a speed equal to half of the shear wave velocity, we add extra stress to the corresponding grids so that their fracture begins. This artificial initial process is usually imposed within the first 20 time steps. On the other hand, the rupture is spontaneously arrested according to the energy balance around the rupture front in the propagation direction, or simply at the end of the model region (virtually surrounded by unbreakable barriers).

3. Simulation Results

We consider two interesting cases, where the rupture begins at the lower continuous part (Model A), or at the upper disconnected segment (Model B). Figures 2 and 3 show snapshots of slip velocity and shear stress on the fault plane during dynamic rupture propagation. In Model A, after the rupture arrives at the bottom of the slit, the rupture front still propagates as a single circular-shaped crack, except for a slight disturbance when it meets the slit. We see that most of the stress change occurs near the crack front. On the other hand, in Model B, we observe that rupture propagation is affected more by the slit. The upper part at segment 2 breaks after the rupture front is redirected by the slit. We observe that the stress wave propagating at the upper part of segment 2 is detached from the crack, which is not large enough to break simultaneously because of the absence of the crack front. The rupture at segment 2 starts as a result of stress concentration realized by the rupture coming from the bottom. Nevertheless, final slip distributions (Figure 4) are very similar in the two cases, because we assign uniform frictional parameters and uniform initial stress field in both cases. Also, the continuity of the fault geometry enables the rupture to cover the whole of the modeled region in spite of differences in the details of the rupture process.

These simple examples imply a very important insight; the size of the rupture area is principally controlled by the continuity of the fault geometry, but rupture directivity at each point is not always dictated by the location of the hypocenter, which is also implied by the seismic inversion results. Final slip distribution is principally determined by the fault geometrical continuity/discontinuity. We find a single asperity at the lower continuous part, whereas there are two at the discontinuous part, because the slip is evidently reduced to zero at the slit. This infers that partial segmentation of the fault might also roughly localize asperities.

Table 1. Model parameters used in this study. We change D_{slit}, W and τ_0 in Section 4 for discussion. 20

rigidity μ	30.0 GPa
P wave velocity V_p	5.57 km/s
grid size Δs	0.5 km
time step Δt	0.045 sec
slit gap D_{slit}	1.0 km
slit width W_{slit}	7.5 km
fault width beneath the slit W	5.5 km
initial shear stress τ_0	6 MPa
peak strength τ_p	10 MPa
critical slip-weakening distance D_c	0.5 m

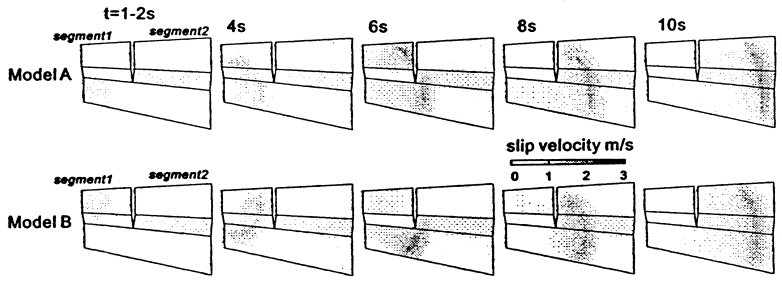

Fig. 2. Snapshots of rupture propagation. They show slip velocity on the fault plane. Rupture begins at the lower continuous part (Model A) and at the upper discontinuous part (Model B).

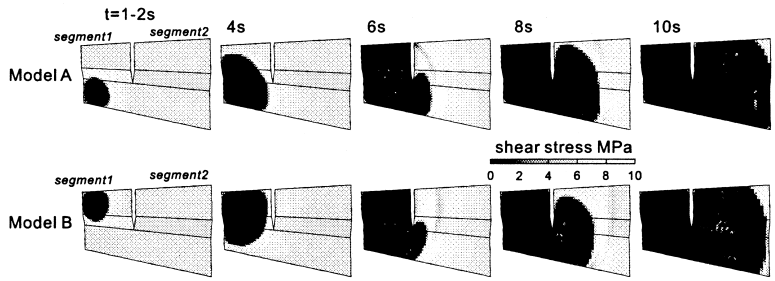

Fig. 3. Snapshots of stress propagation for Model A (hypocenter at the continuous part of the fault plane) and Model B (hypocenter at the discontinuous part). They show shear stress in the x_1 direction on the fault plane.

As we reconsider the 1999 Izmit earthquake based on these results, the continuity at depth beneath Sapanca lake is after all the most important feature of this rupture process in spite of the complexity of the fault geometry near the surface. Most inversion results infer a large asperity to the east of the lake, so it might be reasonable to consider the Sapanca lake as a slit from the point of view of the model we present here.

4. Discussion

4.1 Slit Gap

In the previous simulations, we have seen that the rupture growth depends only on the continuity of the fault system. On the other hand, geological observations imply that rupture does not jump a surface gap greater than 5 km [e.g. Lettis *et al.*, 2002]. Figure 5 shows the simulation result in the case of a slit gap D_{slit} of 5 km. It should be noted that introducing a slit gap of 5 km leads to a geometry with an angle between the two sides of the slit that is wider than in the model presented before. We initiate the rupture at the lower continuous part as in Model A shown in Figure 2. What we see here is the same as in Figure 2. In spite of the large distance between the two sides of the slit, the rupture propagates over the entire fault, because the fault is partially continuous at depth. Even if we assume a slit gap D_{slit} is longer than 5 km, or if we start the rupture in the upper discontinuous part, the rupture reaches all parts of the fault model, as can be seen in Figure 5. We conclude that this kind of fault geometry does not affect the rupture in spite of steep changes in geometry from the lower continuous to the upper discontinuous parts, under uniform initial shear stress and frictional parameters.

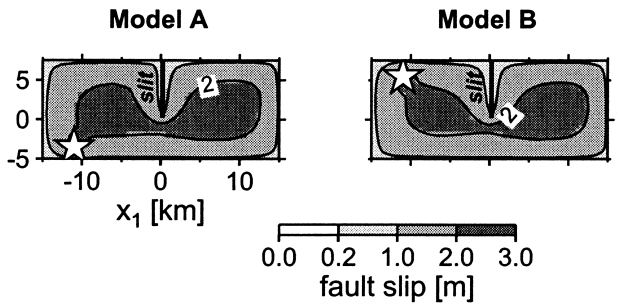

Fig. 4. Comparison of final slip distribution for both models.

The apparent limit of 5 km on the surface as inferred by the geological observations should be explained by other means. Fault geometry may in fact be discontinuous at depth in the same way it is observed on the surface, as demonstrated by Harris and Day (1993, 1999) and by Kase and Kuge (1998, 2001). Or, we have to consider the exact relation between an external stress field and the fault geometry. We can easily imagine that the stress field around the slit is different from the rest of the fault plane. In any case, in future studies, we have to discuss this problem based not only on the surface breaks but also on the fault geometry at depth.

4.2 Degree of Continuity

Next, we change the fault widths beneath the slit W, while keeping the value of W_{slit} to investigate the importance of the relative length of the slit. After several studies on a critical parameter controlling dynamic rupture propagation [e.g. Andrews, 1976 b; Day, 1982; Shibazaki and Matsu'ura, 1992], Madariaga and Olsen (2000) introduced a non-dimensional parameter κ, which can parameterize rupture behavior under the existence of slip-weakening law;

$$\kappa=\frac{\tau_0^2}{\mu\tau_p}\frac{W}{D_c}\cdot \qquad (2)$$

and roughly represents the ratio of the available strain energy ($\sim\tau_0^2 W/\mu$) to the fracture energy ($\sim\tau_p D_c$). All parameters in Equation (2) have been defined before except the characteristic distance W. How to choose W is still under discussion and it may be heterogeneous on a fault system during an earthquake. Madariaga and Olsen (2000) and Peyrat *et al.* (2002) have proposed taking the asperity radius, width of the fault or asperity, or even a hypocentral

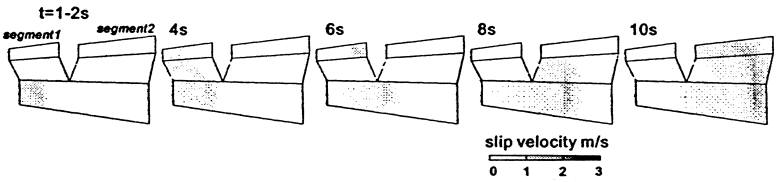

Fig. 5. Snapsot of rupture propagation for D_{slit}=5 km. Rupture begins at the lower continuous part.

distance, to characterize the value of W. The parameter W here should correspond to the fault width beneath the slit W, because we have found that this continuity is a key factor as to whether the rupture progresses further or not. Madariaga and Olsen (2000) reported a critical value of about 0.6 for κ_c based on numerical simulations of a circular crack on a plane and estimated κ_c to be 0.916 analytically. For κ larger than κ_c, rupture can propagate spontaneously. However, we have to note that Madariaga and Olsen (2000) discussed the stability of a rupture, whether or not it can progress spontaneously from an initial asperity, while we discuss the case in which the rupture has already started, but encounters geometrical irregularities along its way.

For parameter κ, the previous cases (Figures 2 and 5) have $\kappa=1.32$, after the parameters given in Table 1. Figure 6 shows final slip distribution for different values of W. In the case where the fault width underlying the slit W is small so the available strain energy underneath the slit is also small in Equation (2), it becomes more difficult for the rupture to propagate on segment 2. We observe that the rupture arrives at all parts on the fault with a W larger than 2 km, which corresponds to $\kappa=0.48$ (the left panel of Figure 6 shows the case of $W=3$ km). On the other hand, the scenario where the rupture ceases to propagate is more complex. It is arrested just beneath the slit at a very small W ($W=0.5$ km for the right panel), whereas it progresses upward at an intermediate value of W ($W=1.5$ km; the middle panel in Figure 6), which is an example in which a small change of fault geometry dynamically affects the rupture process. Each segment has two kinks in the x_2x_3-plane and they did not generally play a large role as can be seen in Figure 5. However, they are important when the rupture front is not mature enough yet, just after passing the slit, as seen in the middle panel of Figure 6. In fact, when we reduce the steepness of these kinks, while keeping $W=1.5$ km, the rupture can continue until the end. This infers that the effective characteristic distance controlling the parameter κ should be larger than the fault width beneath the slit W, including the effect of small differences in fault geometry in the x_3 direction.

4.3 Initial stress and dynamic stress interaction

Although the slit gap is just 1 km in the previous cases, we did not observe any rupture jump between disconnected parts, except at the rupture passage beneath the slit. However, if we assume a higher initial shear stress, the dimensionless parameter κ effectively becomes large (higher available strain energy) so the rupture may progress further. Let us consider the extreme geometry model shown in the right panel of Figure 6, where W of 0.5 km corresponds to $\kappa=0.12$. Figure 7 shows the snapshots of rupture propagation in the case of $\tau_0=8$ MPa ($\kappa=0.21$) and of $\tau_0=9$ MPa ($\kappa=0.27$). In spite of the small κ, the rupture passes underneath the slit and propagates very rapidly everywhere, even at a speed that is faster than the shear wave velocity. This implies the existence of a strong dynamic stress transfer at the bottom of the slit due to the proximity of the two sides of the slit and due to the very high rupture speed as a result of the high initial shear stress. Both effects can create a powerful stress wave propagation beyond the crack,which is sufficient to enhance rupture progress on segment 2.

However, it is still difficult to distinguish whether or not the rupture jumps the slit. In the case

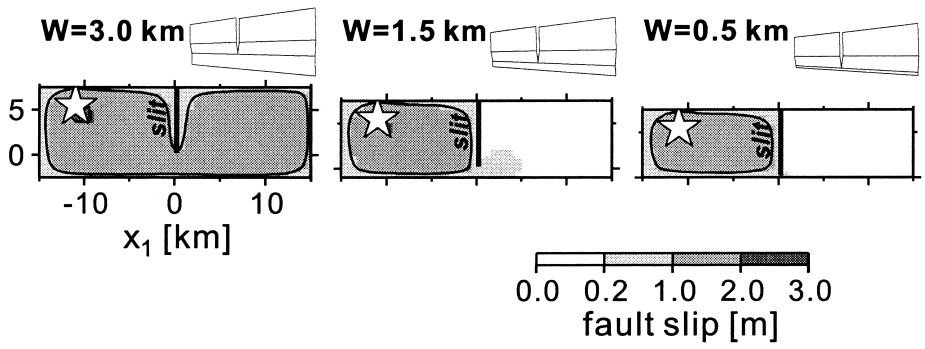

Fig. 6. Final slip distributions for different fault widths beneath the slit W. 3D illustration of fault model is presented at each top-right side.

with $\tau_0=8$ MPa, it clearly goes around the slit. On the other hand, at time step 70 in the case of $\tau_0=9$ MPa, we can observe a vague rupture front beyond the slit. Its form is almost straight and parallel to the slit, so we speculate that this comes directly from over the slit. At the same time, we see a stronger front passing beneath the slit, which enhances the rupture at time steps 80–90. These examples imply that the continuous rupture progress in the continuous part on the fault plane beneath the slit is still more effective than the rupture jump between discontinuous segments. As a result, fault continuity is after all the most significant factor for rupture process.

Through these simulations, we have found that the increase in κ, namely the available strain energy ($\sim\tau_0^2 W/\mu$), qualitatively explains how easily the rupture can propagate over the slit. However, finding the critical κ is not so easy. For example, compared to a rectangular planar fault in 3D [e.g. Madariaga and Olsen, 2000], we might have underestimated the characteristic distance W, which was assumed simply as the width of the continuous part of the fault. It should be more complex as a function of fault geometry, considering the possibility of a dynamic interaction between non-planar faults. This tells us the importance of numerical investigation for a non-planar fault system that is closer to a realistic geological system.

4.4 Geological Implication

We have carried out numerical simulations for a system that is analogous to a strike slip. It should be noted, however, that our model does not include the free surface. The effect of the free surface is expected to enhance the possibility of rupture progress, especially near the surface. Thus, we cannot conclude that rupture always travels by way of the deep portion as in Model B (Figure 2) when we consider a more realistic situation around faults. For a quantitative discussion of observations, we need to pay attention to this limitation. Furthermore, in the field, inelastic deformation or formation of new faults is always possible between the slit, so the whole process should be more complex. Thus we need to know the importance of each factor we neglected in this study.

Through these simulations, we have pointed out the importance of fault geometry for the rupture process, discussing the 1999 Izmit earthquake as an example. For the 1992 Landers earthquake, one of the key issues is the rupture transfer between pre-recognized faults. Through paleoseismic studies by drilling to the faults at several locations, Rockwell *et al.* (2000) found out a preexisting fault that had been unknown until the 1992 rupture, and estimated the times of previous events at each site. This implies that the existing continuity of the fault system at depth may also have led to a global rupture process in this earthquake. The following 1999 Hector Mine earthquake in the same region also has a complexity in its rupture process due to the uncertain fault geometry [Li *et al.*, 2003]. The fault system of this earthquake may have a partial branching structure. This kind of complex fault geometry is not limited to strike-slip faults, but is inferred for inverse faults such as the upper end of the 1994 Northridge earthquake rupture [e.g. Carena and Suppe, 2002] as well.

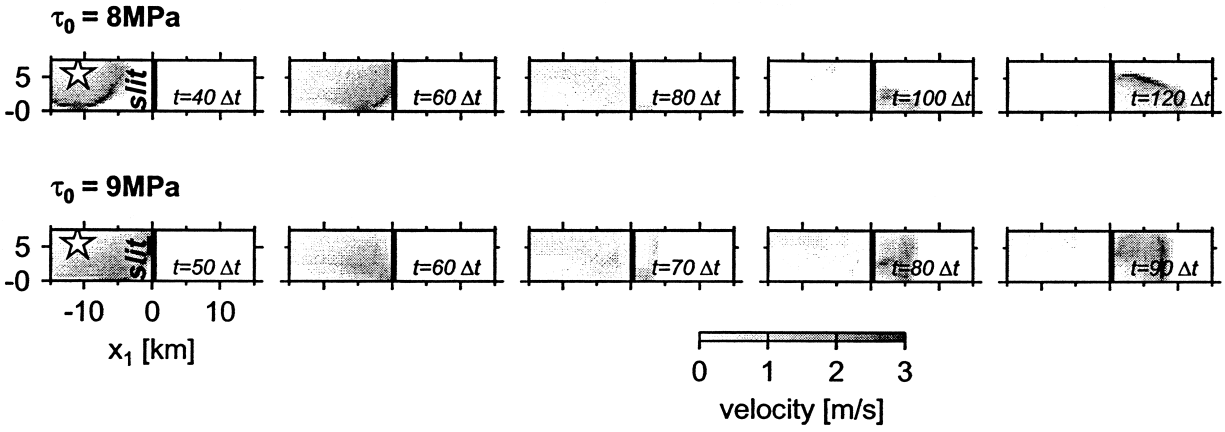

Fig. 7. Snapshots of rupture propagation with an initial shear stress τ_0 of 8 MPa and 9 MPa. Fault geometry is the same as that in the right panel in Figure 6.

Thus, in general, it is important to know the fault geometry at depth when investigating its effect on rupture process and resultant ground motion.

5. Summary

We numerically investigated dynamic rupture propagation on a branched fault, which is partially segmented by a slit. We found that the existence of the slit can significantly effect rupture directivity depending on the relative location of the hypocenter. At the same time, final rupture area and final slip distribution are primarily controlled by the continuity of the fault system at depth regardless of slit gap and details of the rupture process. However, if the continuity is too narrow, the rupture is disturbed. If the stress accumulation is sufficient, the rupture progresses as a result of a powerful dynamic stress transfer at the bottom of the slit. As an extreme case, part of rupture might jump from one segment to the other over the slit. Even in such a case, the massive part of rupture prefers the weakest path, which is beneath the slit.

Acknowledgments

We thank E. Durukal, S. Ide and, and an anonymous reviewer for their comments, which improve this paper. Some part of this work was supported by the project "Special Project for Earthquake Disaster Mitigation in Urban Areas" of Ministry of Education, Sports, Science and Technology, Japan. The numerical simulations were performed on parallel computers at the Département de Simulation Physique et Numérique de l'Institut de Physique du Globe de Paris (IPGP), France and at the Laboratoire de Géologie de l'Ecole Normale Supérieure (ENS) Paris, France.

References

Andrews, J., 1976 a, Rupture propagation with finite stress in antiplane strain, *J. Geophys. Res.,* **81**, 3575–3582.

Andrews, J., 1976 b, Rupture velocity of plane strain shear cracks, *J. Geophys. Res.,* **81**, 5679–5687.

Aochi, H., E. Fukuyama and M. Matsu'ura, 2000, Spontaneous rupture propagation on a non-planar fault in 3D elastic medium, *Pure appl. geophys.,* **157**, 2003–2027.

Aochi, H. and R. Madariaga, 2003, The 1999 Izmit, Turkey, earthquake: Non-planar fault structure, dynamic rupture process and strong ground motion, *Bull. Seism. Soc. Amer., in press.*

Carena, S. and J. Suppe, 2002, 3-D Imaging of active structures using earthquake aftershocks: the Northridge thrust, California, *J. Structural Geology,* **24**, 887–904.

Cochard, A. and R. Madariaga, 1994, Dynamic faulting under rate-dependent friction, *Pageoph,* **142**, 419–445.

Das, S. and K. Aki, 1977, A numerical study of two-dimensional spontaneous rupture propagation, *Geophys. J. R. astr. Soc.,* **50**, 643–668.

Day, S. M., 1982, Three-dimensional simulation of spontaneous rupture: the effect of nonuniform prestress, *Bull. Seism. Soc. Am.,* **72**, 1881–1902.

Fukuyama, E. and R. Madariaga, 1995, Integral equation method for planar crack with arbitrary shape in 3D elastic medium, *Bull. Seism. Soc. Amer.,* **85**, 614–628.

Fukuyama, E. and R. Madariaga, 1998, Rupture dynamics of a planar fault in a 3D elastic medium: rate-and slip-weakening friction, *Bull. Seism. Soc. Amer.,* **88**, 1–17.

Fukuyama, E., T. Tada and B. Shibazaki, 2002, Three dimensional dynamic rupture propagation on a curved/branched fault based on boundary integral equation method with triangular elements, *Eos Trans. AGU,* **83** (**47**), Fall Meet. Suppl., Abstract NG62A-0930.

Harris, R. A. and S. M. Day, 1993, Dynamics of fault interaction: parallel strike-slip faults, *J. Geophys. Res.,* **98**, 4461–4472.

Harris, R. A. and S. M. Day, 1999, Dynamic 3D simulations of earthquakes on en echelon faults, *Geophys. Res. Lett.,* **26**, 2089–2092.

Harris, R. A., J. F. Dolan, R. Hartleb and S. M. Day, 2002, The 1999 Izmit, Turkey earthquake: A 3D dynamic stress transfer model of intra-earthquake triggering, *Bull. Seism. Soc. Amer.,* **92**, 245–255.

Kame, N., J. R. Rice and R. Dmowska, 2003, Effects of prestress state and rupture velocity on dynamic fault branching, *J. Geophys. Res.,* **108**(**B5**), 10.1029/2002 JB 002189.

Kame, N. and T. Yamashita, 1997, Dynamic nucleation process of shallow earthquake faulting in a fault zone, *Geophys. J. Int.,* **128**, 204–216.

Kame, N. and T. Yamashita, 1999, Simulation of the spontaneous growth of a dynamic crack without constraints on the crack tip path, *Geophys. J. Int.,* **139**, 345–358.

Kase, Y. and K. Kuge, 1998, Numerical simulation of spontaneous rupture processes on two non-coplanar faults: the effect of geometry on fault interaction, *Geophys. J. Int.,* **135**, 911–922.

Kase, Y. and K. Kuge, 2001, Rupture propagation beyond fault discontinuities: Significance of fault strike and location, *Geophys. J. Int.,* **147**, 330–342.

Lettis, W., J. Bachhuber, R. Witter, C. Brankman, C. E. Randolph, A. Barka, W. D. Page and A. Kaya, 2002, Influence of releasing step-overs on surface fault rupture and fault segmentation: Examples from the 17 August 1999 Izmit earthquake on the North Anatolian Fault, Turkey, *Bull. Seisme. Soc. Amer.,* **92**, 19–42.

Li, Y.-G., J. E. Vidale, D. D. Oglesby, S. M. Day and E. Cochran, 2003, Multiple-fault rupture of the M7.1 Hector Mine, California, earthquake from fault-zone trapped waves, *J. Geophys. Res.,* **108**(**B3**), 10.1029/2001JB001456.

Madariaga, R. and K. B. Olsen, 2000, Criticality of Rupture Dynamics in 3-D, *Pure appl. geophys.,* **157**, 1981–2001.

Peyrat, S., R. Madariaga and K. B. Olsen, 2002, La dynamique

des tremblements de terre vue à travers le séisme de Landers du 28 juin 1992, *C. R. Mecaniaue,* **330**, 235–248.
Rockwell, T. K., S. Lindvall, M. Herzberg, D. Murbach, T. Dawson and G. Berger, 2000, Paleoseismology of the Johnson Valley, Kickapoo, and Homestead Valley Faults: Clustering of Earthquakes in the Eastern California Shear Zone, *Bull. Seism. Soc. Amer.,* **90**, 1200–1236.
Shibazaki, B. and M. Matsu'ura, 1992, Spontaneous processes for nucleation, dynamic propagation, and stop of earthquake rupture, *Geophys. Res. Lett.,* **19**, 1189–1192.
Tada, T., E. Fukuyama and R. Madariaga, 2000, Non-hypersingular boundary integral equations for 3-D non-planar crack dynamics, *Comp. Mech.,* **25**, 613–626.
Tada, T. and T. Yamashita, 1997, Non-hypersingular boundary integral equations for two-dimensional non-planar crack analysis, *Geophys. J. Int.,* **130**, 269–282.

(Received December 13, 2002)
(Accepted May 8, 2003)